ORIGINAL PAPER

In silico evaluation of flavonoids as potential inhibitors of SARS-CoV-2 main nonstructural proteins (Nsps)—amentoflavone as a multitarget candidate

Andrés Portilla-Martínez[1] · Miguel Ortiz-Flores[1] · Isabel Hidalgo[2] · Cristian Gonzalez-Ruiz[3] · Eduardo Meaney[1] · Guillermo Ceballos[1] · Nayelli Nájera[1]

Abstract

Despite the development of vaccines against COVID-19 disease and the multiple efforts to find efficient drugs as treatment for this virus, there are too many social, political, economic, and health inconveniences to incorporate a fully accessible plan of prevention and therapy against SARS-CoV-2. In this sense, it is necessary to find nutraceutical/pharmaceutical drugs as possible COVID-19 preventives/treatments. Based on their beneficial effects, flavonoids are one of the most promising compounds. Therefore, using virtual screening, 478 flavonoids obtained from the KEGG database were evaluated against non-structural proteins Nsp1, Nsp3, Nsp5, Nsp12, and Nsp15, which are essential for the virus-host cell infection, searching for possible multitarget flavonoids. Amentoflavone, a biflavonoid found mainly in *Ginkgo biloba*, *Lobelia chinensis*, and *Byrsonima intermedia*, can interact and bind with the five proteins, suggesting its potential as a multitarget inhibitor. Molecular docking calculations and structural analysis (RMSD, number of H bonds, and clustering) performed from molecular dynamics simulations of the amentoflavone-protein complex support this potential. The results shown here are theoretical evidence of the probable multitarget inhibition of non-structural proteins of SARS-CoV-2 by amentoflavone, which has wide availability, low cost, no side effects, and long history of use. These results are solid evidence for future in vitro and in vivo experiments aiming to validate amentoflavone as an inhibitor of the Nsp1, 3, 5, 12, and 15 of SARS-CoV-2.

Keywords SARS-CoV-2 · Non-structural protein · Docking · Molecular dynamics · Multitarget · Amentoflavone

Miguel Ortiz-Flores and Nayelli Nájera are co-senior authors of this work.

✉ Nayelli Nájera
nnajerag@ipn.mx

1 Sección de Posgrado, Escuela Superior de Medicina, Instituto Politécnico Nacional, Plan de San Luis Y Diaz Mirón S/N, Col Santo Tomás, 11340 Mexico City, Mexico

2 Laboratorio de Investigación en Inmunología Y Salud Pública, Facultad de Estudios Superiores Cuautitlán, Unidad de Investigación Multidisciplinaria Universidad Nacional Autónoma de México, Estado de México, Mexico City, Mexico

3 Facultad de Estudios Superiores Iztacala, Universidad Nacional Autónoma de México, Mexico City, Mexico

Introduction

The recent severe acute respiratory syndrome coronavirus 2 (SARS-CoV-2) pandemic that began in Wuhan (China) has expanded worldwide with an estimated 539,893,858 confirmed cases and 6,324,112 deaths on June 23, 2022, worldwide [1]. This virus causes coronavirus disease 2019 (COVID-19), whose clinical manifestations are not specific but somewhat like many viral illnesses [2]. The most common symptoms after viral incubation between 4 and 14 days are cough, fever, fatigue, anosmia, dysgeusia, headache, and sometimes nausea and diarrhea [3]. Clinical manifestations can range from mild to very severe and even fulminant disease [3]. Pandemic has promoted several strategies in all science branches to understand and solve COVID-19 conditions. Vaccine development is one of the main strategies adopted by different research institutes and pharmaceutical companies. At this moment, at least six vaccines have

concluded the clinical trial phase III and are approved worldwide for emergency use [4].

Nevertheless, vaccines have less than 95% efficacy, depending on age and comorbid-mortality factors of the population. In addition, due to the short development time and technological novelty adopted, these vaccines have been deployed with several unresolved issues such as technical problems associated with the production of billions of doses and ethical issues related to the availability of these vaccines in the poorest countries [5]. In addition, the SARS-CoV-2 virus is evolving fast, and there is no complete guarantee that vaccines will protect the population against new virus variants [6]. Furthermore, political, economic, and social (vaccine mistrust, asymptomatic individuals (30%), and not following security methods) constraints may limit vaccine access [5].

Drug development for COVID-19 disease treatment continues to be necessary. Several investigational drugs, aiming to inhibit viral entry into the host mechanisms and thus block subsequent viral replication, are currently explored in clinical trials. An example is remdesivir [7], which the Food and Drug Administration (FDA) approved for COVID-19 treatment requiring hospitalization in patients 12 years of age and older. Several drugs must complete clinical trials phase II and III to be approved [8]. So, it is still a long way to have fully approved drugs to treat and prevent this disease.

SARS-CoV-2 possesses potential targets for developing new drugs; some are the family of non-structural proteins (Nsps), which are essential macromolecules involved in the viral genome replication and transcription. Sixteen Nsps have been identified, participating in different host cell infection processes [9].

The viral proteases Nsp3 (PLPro) and Nsp5 (MPro) cleave proteolytically viral polyproteins to form the rest of the Nsps. Most of them integrate the machinery of the replication/transcription complex, highlighting the role of Nsp12 (RdRp) as an RNA-dependent polymerase that in complex with Nsp7 and Nsp8 greatly stimulates polymerase activity; and Nsp15 (EndoU) an endoribonuclease which helps the virus evades the immune system, preventing the detection of viral dsRNA by the host. Furthermore, Nsp1 interferes with the host cell protein synthesis, binding to the 40S ribosomal subunit and endonucleolytic cleavage of host mRNA [9].

In this sense, it is mandatory to continue the research to find and develop nutraceutical/pharmaceutical (easy to insert in our diets or of feasible acquisition) directed to inhibit these important proteins for COVID-19 treatments, such as flavonoids. Flavonoids are molecules with variable phenolic structures widely distributed in the plant kingdom; they are found in leaves, seeds, roots, stems, fruits, and barks [10]. These molecules are considered promising biologically active substances to prevent SARS-CoV-2 due to their possible beneficial action in different mechanisms of this virus

infection: inhibiting essential enzymes for virus replication and regulation of immune system functions [11].

Amentoflavone ($C_{30}H_{18}O_{10}$) belongs to the flavonoid family (a C3′-C8″ apigenin dimer). *Ginkgo biloba*, *Lobelia chinensis*, and *Byrsonima intermedia* are some plants where amentoflavone can be found; all have been used in traditional Chinese or American medicine [12]. Among the biological effects associated with the use of amentoflavone are anti-inflammatory [13, 14], antifungal activity [15], effects on the nervous system [16] and the cardiovascular system [17], and antiviral effects [11]. These facts made amentoflavone an excellent candidate for interacting and possibly modulating different target proteins of SARS-CoV-2 virus.

In the present work, we use one of the important parameters that are currently part of the rational drugs design process, such as the ability to predict ΔG (free energy) binding values, since the affinity of a drug for any receptor is closely related to its biological activity. We use molecular dynamics to predict amentoflavone's structural dynamics, stability, and binding affinity and predict the feasibility of using it as a SARS-CoV-2 non-structural protein (Nsp1, 3, 5, 12, and 15) inhibitor.

Methods

Protein preparation

Crystal structures of non-structural protein 1 from SARS-CoV-2 structure were obtained from Zhang lab server https://zhanggroup.org/COVID-19/, ID: QHD43415_1 [18]; the structures of SARS-CoV-2 papain-like protease (PLPro) with inhibitor GRL0617 (PDB ID: 7JRN) [19], SARS-CoV-2 3CL protease (3CL pro) in complex with a novel inhibitor (PDB ID: 6M2N) [20], SARS-Cov-2 RNA-dependent RNA polymerase in complex with cofactors (PDB ID: 6M71) [21], and crystal structure of Nsp15 endoribonuclease form SARS-CoV-2 in complex with potential repurposing drug tipiracil (PDB ID: 6WXC) [22] were downloaded from the Protein Data Bank database (https://www.rcsb.org/) [23] and were prepared in USCF Chimera [24], removing water atoms, co-crystallized ligands, cofactors, and/or extra chains from each structure; furthermore, each designed protein was minimized energetically with conjugate gradient and steepest descent algorithms of this software, using AMBER ff14SB force field. The structures were subjected to 100 ns of molecular dynamics, according to method further described, and 200 ns in the case of Nsp1, to understand its conformational profile; after dynamics completion RMSD and cluster analysis were performed to obtain the main structure or/and the pdb files for the most representative clusters; after that, proteins structure were saved in pdbqt format in

AutoDock Tools [25] after adding polar hydrogens and Kollman charges to perform virtual screening assay.

Ligand preparation

A specific search was performed on the advanced module of the PubChem database, using "flavonoid" as keyword in the phytochemical compound subclassification of the KEGG database. KEGG is a comprehensive drug information resource for approved drugs in Japan, the USA, and Europe, unified based on active ingredients' chemical structure and/ or chemical components [26].

On the other hand, 3D conformer of co-crystallized ligands was separated from its protein: GRL0617 for Nsp3, baicalein from Nsp5, for Nsp12 the novel AT9 inhibitor was obtained from PDB ID: 7ED5 [27], tipiracil for Nsp15, and no ligand for Nsp1, because no structures with co-crystallized ligand(s) are available for this protein. In the same sense, the 3D conformers of the 478 flavonoids found were downloaded in sdf (structure data file) format and converted to pdb (protein data bank) using the module of OpenBabel software [28], applying the conjugate gradient and steepest descent algorithms for energy minimization using Universal Force Field (UFF). The energy minimized structures were converted to pdbqt format by the AutoDock Tools script prepligand4.py included in the software package [25].

Virtual screening

For the virtual screening, a directed methodology was employed, with the grid box centered on each protein catalytic site (based on co-crystallized ligand), covering a $20 \times 20 \times 20$ Armstrong volume on each. AutoDock Vina virtual screening script written in Linux Shell was used to perform this process [29], generating a single docking pose, which were analyzed based on protein–ligand interactions and binding affinity values.

Molecular docking

Results of virtual screening analysis, amentoflavone was only the molecule showing interactions with nearly all the Nsps; for this reason, this flavonoid was selected as a possible multitarget drug. The amentoflavone molecule was processed with AutoDock Tools to add the polar hydrogens and Gasteiger charges. The grid box dimension used in this section was the same as described above. The amentoflavone vs. Nsps docking was performed with AutoDock Vina with 1000 independent replicates using a script written in Shell to evaluate the best pockets and how the compounds are arranged in them. Afterward, based on AutoDock Vina energy scores and the root-mean-square deviation (RMSD) calculation, the most probable conformation and interaction

site was chosen. With these coordinates, molecular dynamic (MD) simulations were carried out to explore the structural and conformational stability of protein–ligand complexes. Docking methodology was validated by performing independent assays for the co-crystallized ligands. 2D interactions images were built with Discovery Studio [30]. Ligand efficiencies (*LE*) were estimated using the previous reported equation [31] where the *Kd* (dissociation constant of a ligand–protein complex) calculated values by the formulas:

$$Kd = e - \frac{\Delta G}{RT}$$

$$LE = -\frac{RT}{NHA} ln(Kd)$$

where ΔG corresponds to binding energy (kcal mol^{-1}) obtained from docking, R is the gas constant (0.001987207 kcal mol^{-1} K^{-1}), T is the temperature at standard conditions of aqueous solution (298.15 K), and *NHA* denotes the number of non-hydrogen atoms in a ligand.

Molecular dynamics

Protein and protein–ligand complexes were subjected to molecular dynamics using the CHARMM36-jul2020 force field in GROMACS 5 [32, 33], also for amentoflavone and co-crystalized ligands the topologies were generated using CGenFF online server (https://cgenff.umaryland.edu/). Before system solvation using simple point charge (SPC) and TIP3P water model in a cubic box with a minimum distance of 1 nm from the edge of the protein with periodic conditions, the solvent molecules were replaced with NaCl 0.15 M and then neutralized with the necessary counter ions. The solvated systems were minimized using the steepest descent function for 50,000 steps with a maximum force of 10 kJ mol^{-1}. Then, the systems were balanced in the NVT ensemble for 100 ps followed by equilibration in the NPT ensemble for an additional 100 ps with protein and ligand position restraint. Finally, production dynamics were carried out in the NPT ensemble for 100 ns at 300 K and 1 atm pressure using the V-rescale temperature coupling method and Parrinello-Rahman coupling method, respectively. The particle mesh Ewald method was used for computing long-range electrostatic interactions with a non-bonded cutoff of 10 Å and the LINCS algorithm. The non-bonded interactions, Coulomb (electrostatic potential), and Lennard Jones (Pauli repulsion and hydrophobic/van der Waals attractions) interactions were truncated at 10 Å using the Verlet cut-off scheme. The leap-frog algorithm was used to compute the equation of motion with a time step of 2 fs. All the parameters used to perform the molecular dynamics were based on the widely used methodology of Justin Lemkul, which is

constantly updated according to the technological and algorithmic advances of these methods [34].

For the analysis, from all the trajectories, the root mean square deviation (RMSD) of the complex, the protein, and ligand was calculated using the initial ligand and Nsp structures as reference protein and the Cα from the backbone. The number of hydrogen bonds was also calculated between protein and ligand, the most representative (repeated) conformational structures (clusters) with a distance limit of 0.25 nm were obtained, electrostatic and van der Waals interaction energy were computed, and solvent accessible surface area (SASA) also were obtained. GROMACS package was used for all cases. Images were built using PyMOL [35].

Ligand–protein interactions

Interaction fingerprints of protein–ligand complexes were generated by Prolife software [36], using whole molecular dynamics trajectories and graphing those with more than 0.1 ns of occurrence.

Results and discussion

Protein molecular dynamics

RMSD and cluster analysis

After molecular dynamics completions, the stability of Nsp1 (Fig. 1A) and for the rest of the non-structural proteins

(Fig. 1B–E), relative to its conformation was determined by the deviations produced during its simulation (RMSD). The smaller the deviations, the more stable the protein structure. In the same sense, cluster analysis was performed to find the main structure conformation, based on their time frequency along the whole trajectory (Table 1).

Regarding Nsp1, its trajectory has a sudden movement at the beginning (0 to ~0.75 nm), keeping ~0.75 nm as the mean value; however, fluctuations were visible throughout the simulation, like the variation of ~0.25 nm in ~150 ns of the DM simulation. We can appreciate that the protein keeps a main conformation between ~80 and ~104 ns, which corresponds to the structure of cluster 1. In a similar way, correlation of RMSD with the main structures of cluster analysis, it is possible to distinguish cluster 2

Table 1 Results of cluster analysis of the molecular dynamics of the five non-structural proteins

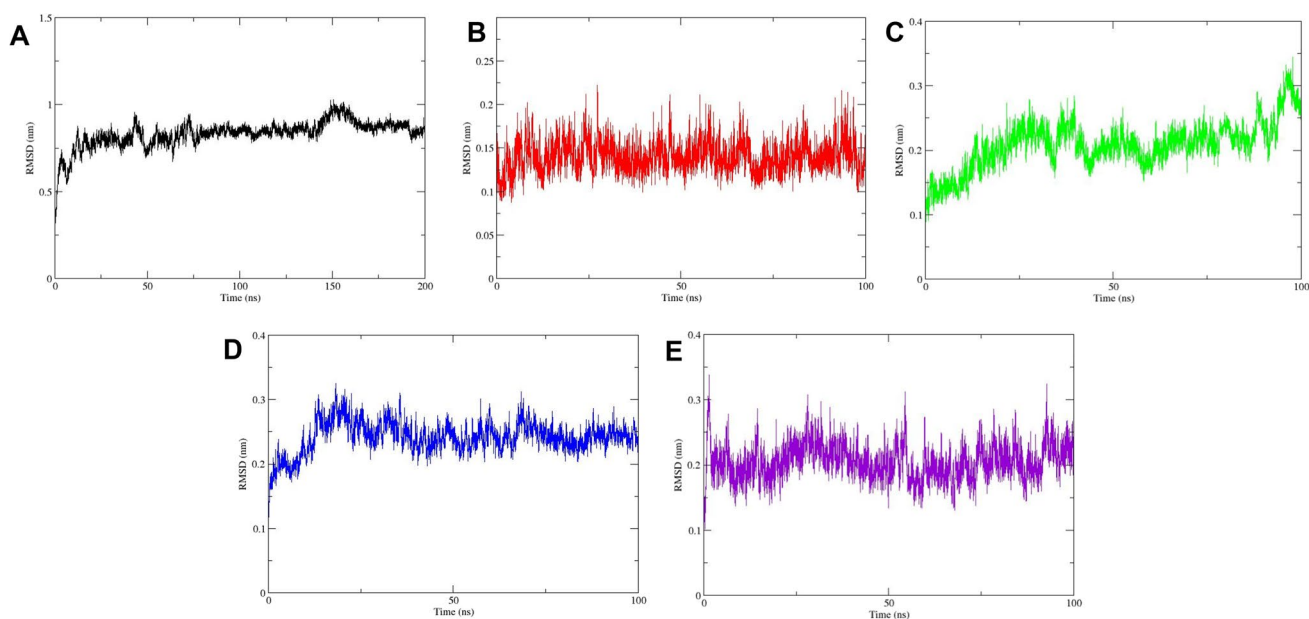| Protein	Cluster (0.25 cutoff)	Cluster frequency (ns)
Nsp1	1	19.2
	2	15.72
	3	11.70
Nsp3	1	97.29
Nsp5	1	87.26
	2	11.38
Nsp12	1	99.76
Nsp15	1	96.92

Fig. 1 The RMSD plot of the five non-structural proteins **A** Nsp1 after 200 ns of molecular dynamics, and 100 ns of molecular dynamics for **B** Nsp3, **C** Nsp5, **D** Nsp12, and **E** Nsp15

from the ~ 170 to ~ 190 ns and cluster 3 from the ~ 105 to ~ 130 ns. Based on the protein structure and the RMSD analysis, we can conclude that relatively large motions over time are due to the inherent flexibility of the structure, mainly in the last fifty residues of the protein, which do not possess a stable secondary structure (i.e., α-helix or β-strand).

On the other hand, RMSD analysis of Nsp3 (Fig. 1B), Nsp12 (Fig. 1D), and Nsp15 (Fig. 1E) shows a more stable protein throughout the simulation, except for the first ns RMSD jump of Nsp15 (~ 0.3 nm). We can notice that Nsp12 (Fig. 1D) reaches a stable conformation approximately at ~ 20 ns; at this point the three proteins fluctuate between the same range all along and without movements that exceed ~ 0.05 nm from each other, except for a few moments of their trajectory, where peaks that stand out (from ~ 0.2 to ~ 0.3 nm) are observed and then return to the movement trend until the end. Based on this, and according to the cluster analysis, the three proteins keep a main structure along the whole trajectory (Table 1).

Finally, according to RMSD analysis of Nsp5 (Fig. 1C), protein stabilizes after ~ 25 ns of the molecular dynamics, at that point and before ~ 80 ns, the protein has no important fluctuations greater than ~ 0.05 nm, the main structure of this period of time corresponds to cluster 1; after ~ 80 ns and until the end of the simulation, protein flexibility have important changes > ~ 0.1 nm, generating a different conformation which is represented by the cluster 2.

In brief, Nsp3, Nsp12, and Nsp15 have a cluster which occupancy is on more than 95% of the dynamics, so this structure was selected for the subsequent analysis; on the other hand, Nsp1 and Nsp5 showed three and two clusters, respectively, the structures of these conformations were considered for the later analysis, taking into account that they represent different conformational states of the protein, and thus can be important to characterize ligand–protein interaction at each conformation.

Virtual screening

Virtual screening was performed with the 478 flavonoids obtained from the search in the KEGG database of PubChem, to determine a possible mechanism by which these flavonoids act on the SARS-CoV-2 Nsp1, 3, 5, 12, and 15 main structures; as mentioned above, the coordinates for virtual screening were centered on each protein catalytic site, based on that from the co-crystallized ligands (Nsp3, 5, 12, and 15) and in case of Nsp1, centered on the alpha carbon of His165, known as an important residue for its activity [37–39].

The distribution of all tested compounds energies for each cluster is represented in Fig. 2, after analysis of the results and seeking for a ligand that interacted with the five proteins to consider it as a probable multitarget flavonoid onto the 10 compounds with the highest binding score (Fig. 3), amentoflavone (Fig. 4) was the only flavonoid that binds with an
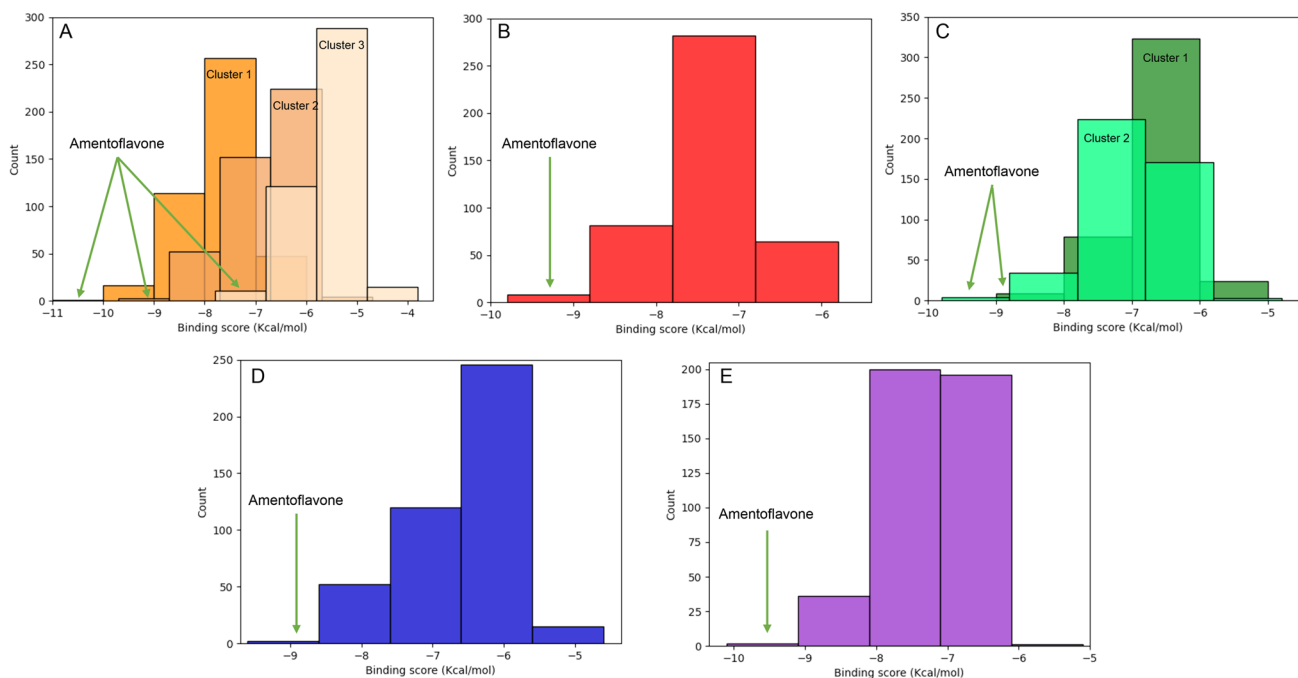

Fig. 2 Energy distribution after virtual screening of the 478 flavonoids with the five non-structural proteins at their respective cluster **A** Nsp1, **B** Nsp3, **C** Nsp5, **D** Nsp12, and **E** Nsp15
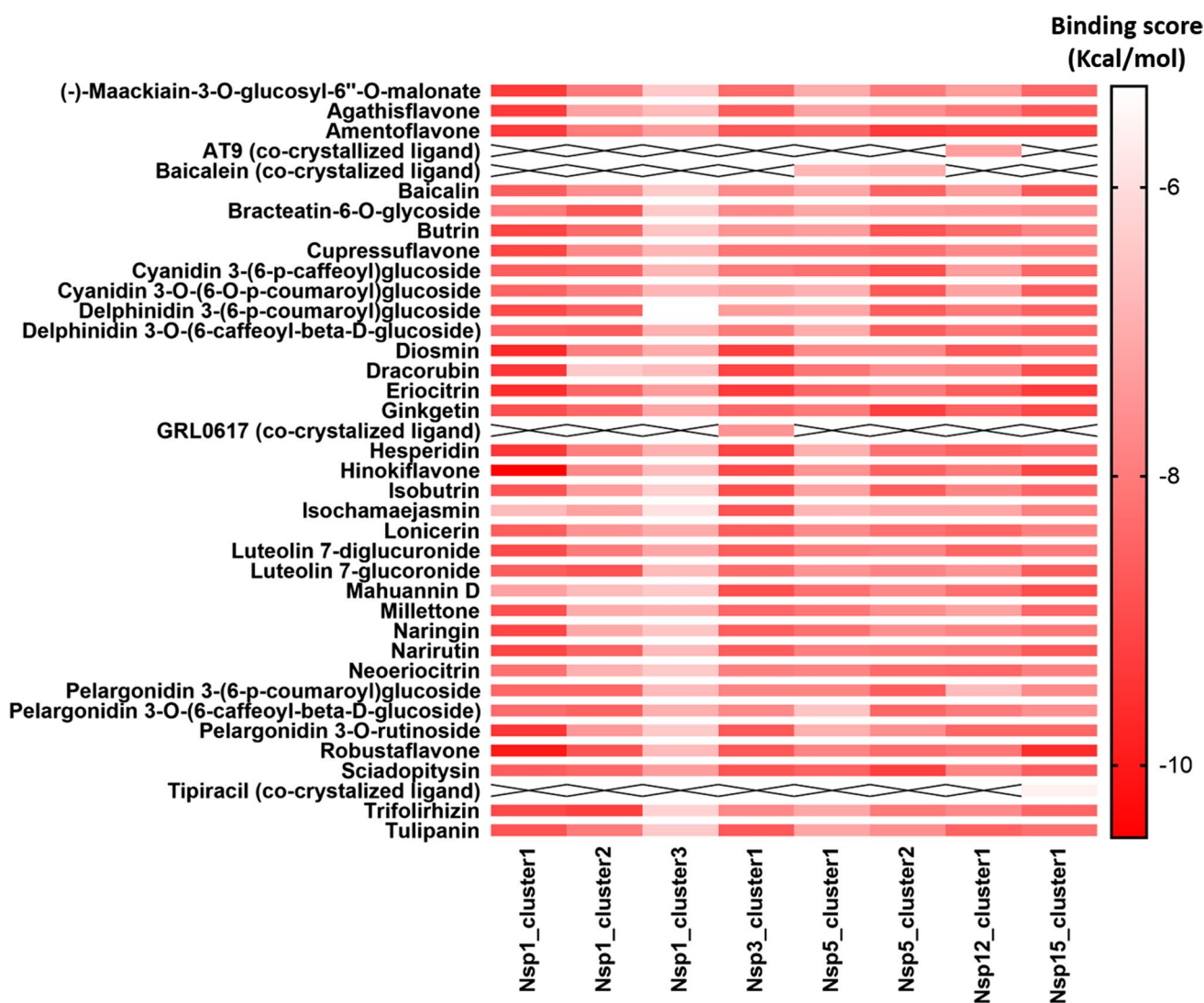
Fig. 3 Binding energy of the best ten molecules and co-crystallized ligands of each protein

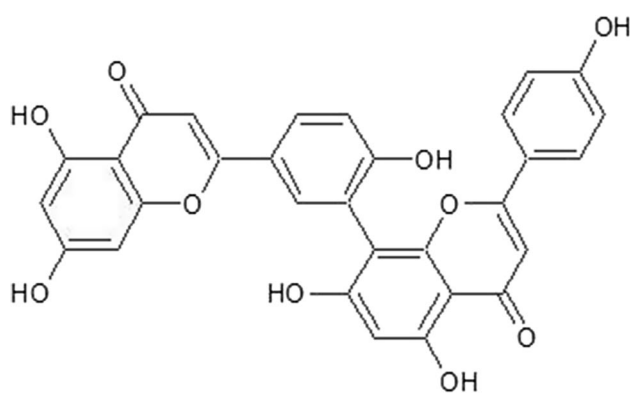acceptable binding score (between − 7.3 and − 9.6 kcal/mol) to the five non-structural proteins.

Fig. 4 Amentoflavone molecular structure

Molecular docking

Based on docking results, Fig. 5A shows the main residues (including those well-described residues important for the enzymatic activity of each protein) involved in the inter-action between amentoflavone and Nsp1, 3, 5, 12, and 15, showing the potential of this molecule as a probable inhibitor; our analysis also shows the two most probable complex conformations based on frequency and RMSD calculations (Fig. 5B). The most frequent cluster, the one with the highest binding energy, was used to perform molecular dynamics studies and the second more frequent cluster represents an alternative binding pose with similar binding score values; data used for this analysis could be found in Table S2.

Analyzing the interactions of each Nsp1 cluster and amentoflavone (Fig. 6A–C), we can see that binding pockets
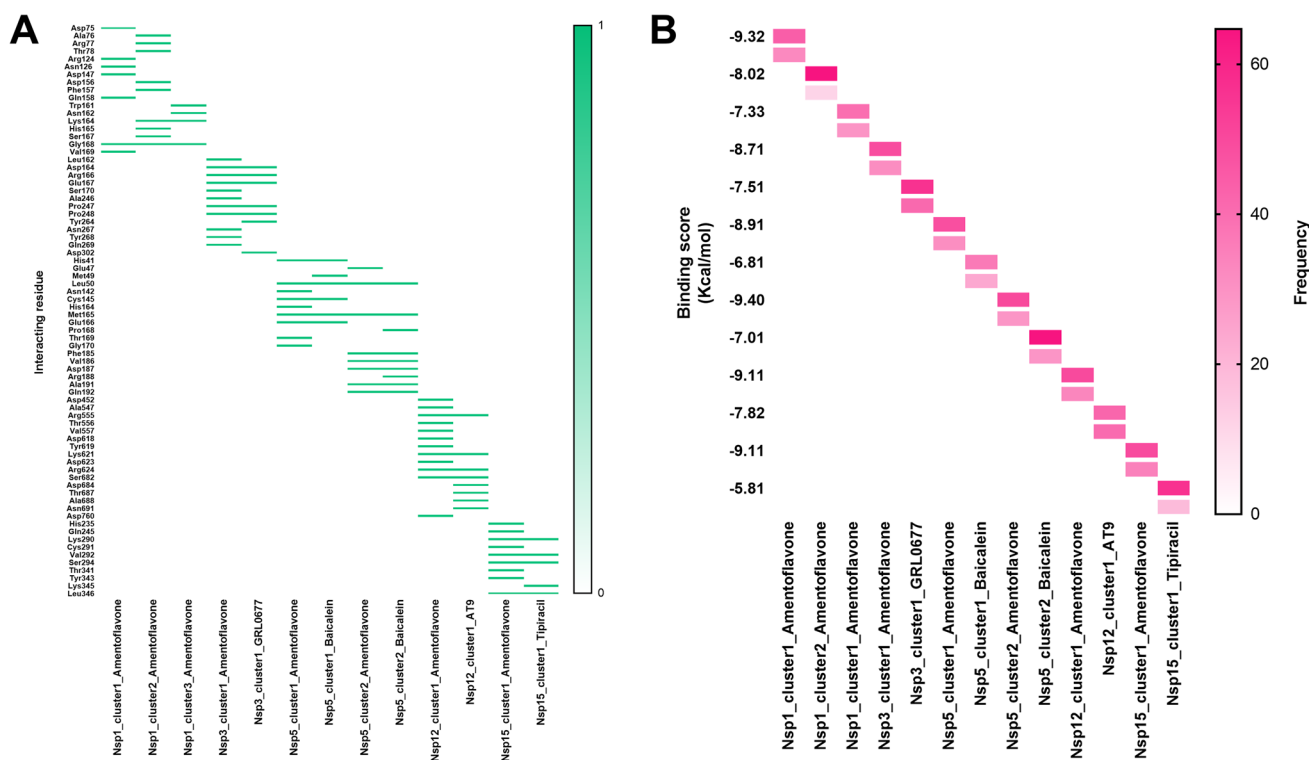
Fig. 5 **A** Main and reported residues important for activity of each protein involved in the interaction between amentoflavone and the five Nsps. **B** Frequency and binding score of the two most probable complex conformations

are different for the three clusters, and so the residues that interact with the ligand. In all cases, the binding pocket of amentoflavone includes residues of the flexible C-terminal region of the protein. For the cluster 1 (Fig. 6A), important interactions include the H-bonds with Arg124 and Gln158, π interactions with Asp75 and Gly168 (Fig. 4A1); it has been demonstrated that Arg124 strongly interacts with the phosphate backbone of SARS-CoV-2 RNA 5′-untranslated region and also Asp75 sometimes formed hydrogen bonds with the bases of it [40], furthermore protein uS5 of the 40S ribosome subunit interacts within a hydrophobic surface which involves this residue and other adjacent ones, including Gln158 and Gly168 [41]. In the case of cluster 2 (Fig. 6B), we can appreciate in Fig. 4A2 that more H-bonds were formed compared to the previous cluster, standing out the interactions with Phe157 and Gly168 which are included in the hydrophobic surface above mentioned [41]. Finally for cluster 3 (Fig. 6C), hydrogen bonds are still being present, now with Asn162 and Gly168, which are part of this important site for the interaction of the 40S ribosome subunit, as well as Trp161; moreover, a π-alkyl interaction is formed with Lys164 an important residue which is crucial for RNA cleavage and translation inhibition functions of SARS-CoV-2 [37–39]. In this sense, amentoflavone could

abolish 40S binding and relieve translational inhibition, by the interactions described above, mainly formed with the residues of the region where the 40S subunit binds.

On the other hand, although Nsp3 is well known for its protease activity cleaving the viral polypeptide, it has also been observed that has an additional function stripping ubiquitin and interferon-stimulated gene 15 (ISG15) from host-cell proteins to aid SARS-CoV-2 in its host evasion innate immune responses (ISG15) [42, 43]. Two active sites blocking this protein activity have been reported: (1) the catalytic site which contains a canonical cysteine protease catalytic triad (Cys111, His272, and Asp286) and (2) the flexible loop BL2 or β-turn, an important mobile loop (Gly266–Gly271) adjacent to the active site that closes upon substrate and/or inhibitor binding [44]. Nevertheless, the cysteine protease drug-like inhibitors present several challenges, notably, for their toxicity and lack of specificity, due to untargeted cysteine residue covalent modification. For that, BL2 loop it is a better option to find probable non-covalent inhibitors, such as the already known compound GRL0617 [45]; the binding of this compound induces BL2 loop closure clamping the inhibitor to the body of the protein, limiting the catalytic triad movement and restricting access to the cysteine by reducing agents, thereby generating an inactive enzyme;
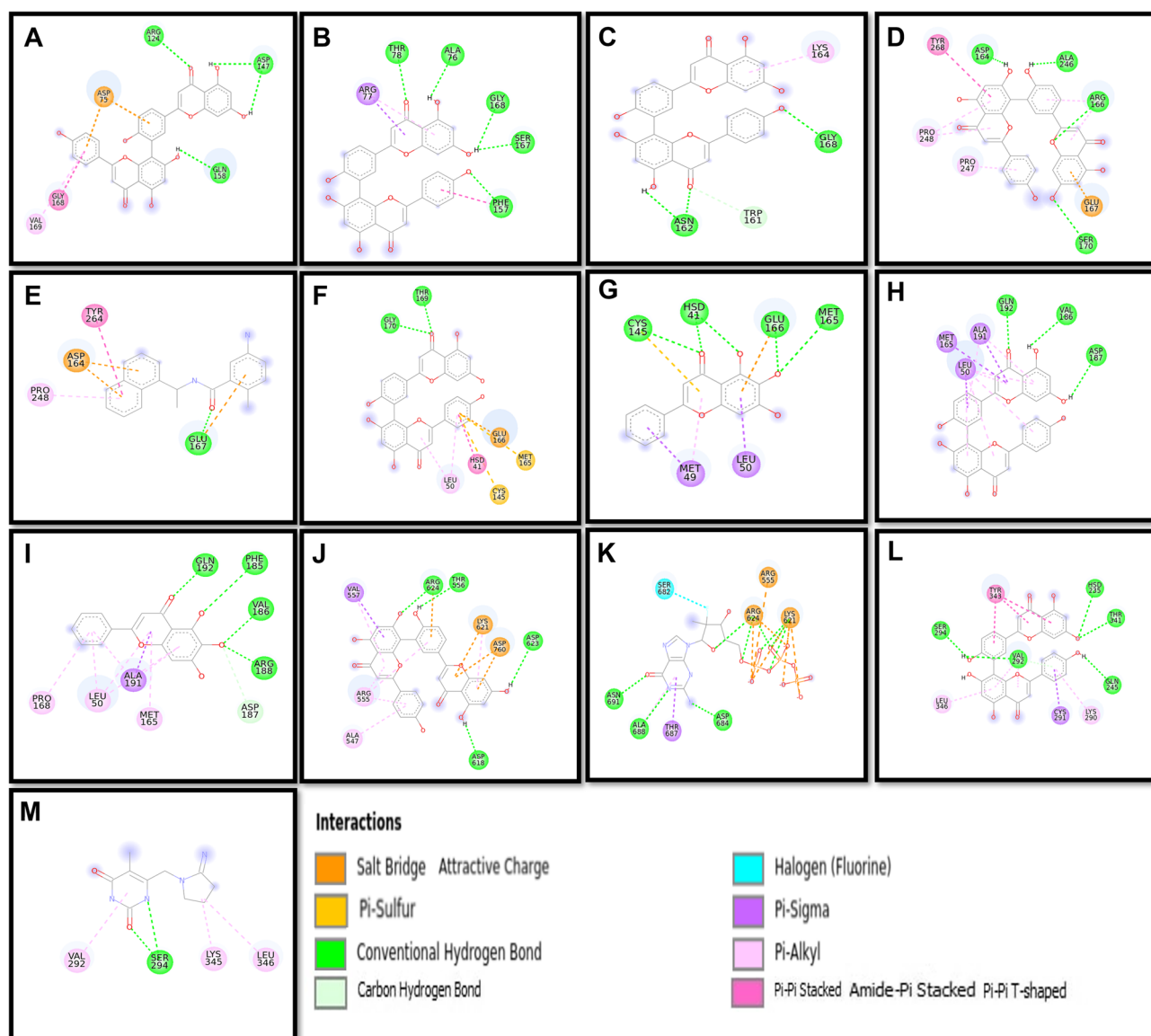
Fig. 6 Molecular docking 2D representation. Each quadrant shows the binding site and the interactions of the results performed with amentoflavone and the co-crystallized ligands vs. all Nsps after the virtual screening. **A** Nsp1_1-amentoflavone, **B** Nsp1_2-amentofla-vone, **C** Nsp1_3-amentoflavone, **D** Nsp3-amentoflavone, **E** Nsp3-GRL0617, **F** Nsp5_1-amentoflavone, **G** Nsp5_1-baicalein, **H** Nsp5_2-amentoflavone, **I** Nsp5_2-baicalein, **J** Nsp12-amentoflavone, **K** Nsp12-AT9, **L** Nsp15-amentoflavone, and **M** Nsp15-tipiracil

also other inhibitor-independent motions are observed at the tip of the fingers domain, which may account for PLpro's ability to interact with topologically different poly-Ub chains and the UBL modifier ISG15 [45, 46]. Reported interactions between GRL0617 and Nsp3 include the residues: Asp164, Gln269 (hydrogen bonds), Tyr264, Tyr268, Pro247, Pro248, Thr301, Arg166 (aromatic interactions) [47]; important interactions coincide with those in Fig. 6E and are comparable with those established with amentoflavone.

As shown in Fig. 6D, amentoflavone forms a hydrogen bond with Asp164, an interaction presumed to be important for ligand stabilization, which is complemented with

the Tyr268 interaction, presumed to make a fitting induced movement to adopt a closer conformation, strengthen the interaction with the inhibitor and anchoring it to the binding site, and with Arg166 and Glu167, important for water and carbonyl coordination [46, 47]. Amentoflavone also interacts with the hydrophobic pocket residues formed by Pro247, Pro248, and Tyr268, which is a specific site for leucine side chain of LXGG consensus sequence recognition [44], for PLPro proteolytic cleavage activity.

In this sense, amentoflavone is a good candidate inhibitor because it binds to this site, making hydrophilic interactions with Nsp3 surface residues and interfering with

the peptide recognition motif LXGG. Furthermore, our results show a binding score of amentoflavone against Nsp3 of -8.69 ± 0.02 kcal/mol, comparable with other studies where this interaction is also addressed: -7.5 kcal/mol for Nsp3 (PDB ID: 6W02) [48] and -8.8 kcal/mol for PLPro (PDB ID: 7JN2) [49]; for this reason, amentoflavone has the advantage that not only inhibiting viral replication but also inhibiting the signaling cascades dysregulation in infected cells.

For the case of Nsp5 or 3CLpro, its catalytic site is composed by a dyad of Cys145 and His41 residues which are buried in an active site cavity located on the protein surface. This cavity consists of S1 to S4 subpockets crucial for substrate recognition; the active site is well characterized, and most crystallized ligands bound to Nsp5 (185 ligands known, including baicalein co-crystallized ligand of the protein used here) coincide at this site, which is comprised by the residues: Thr25, His41, Met49, Asn142, Ser144, Cys145, His163, His164, Gln189, Glu166, Pro168, His172, and Ala191 [50, 51]; our baicalein docking result with Nsp5 cluster1 (Fig. 6I) shows H-bond interaction with the catalytic dyad (Cys145 and His41), Met165 and Gly166, and π-sigma interaction with Met49 and Leu50, which seems to stabilize the molecule into the substrate-binding pocket core (through S1 and S2 subsites). In the case of cluster 2 (Fig. 6H), no interactions with the catalytic dyad were formed, in seems that ligand was pushed out of catalytic site (found in S1 subsite) and displaced to the long loop (residues 185–200), forming interaction with at least five residues of this region, and the S2 subsite, which includes the interactions with Met165 and Pro168; this could be interesting due to the orientation of this loop and II and III domains is important for maintaining a catalytically competent activity [52].

Similarly, our results show that amentoflavone can bind within the active site cavity of cluster 1 (Fig. 6F), carbonyl groups make hydrogen bonds with Thr169 and Gly170 and π electrons mediated interactions with the residues of catalytic dyad (Cys145 and His41) and surrounding amino acids, stabilizing molecule into the substrate-binding pocket core (through S1 and S2 subsites); moreover, the Leu50 side chain also established π-alkyl interaction from the residue nitrogen to the phenyl ring centroid, and Met165 contacted the middle amentoflavone ring via π-sulfur interaction. Talking about cluster 2 (Fig. 6G), a similar displacement, maybe provoked by a closer status of S1 subsite, as occurs with baicalein happened: amentoflavone was pushed to the limits of S2 subsite and the long loop, forming hydrogen bonds and π-sigma interactions, like those formed by baicalein. The interactions at this site could define a possible new target for a possible mechanism of the enzyme inhibition, due to the orientation of this region is important for a competent catalytic activity [52].

Considering the described results, amentoflavone is a great inhibitor candidate for Nsp5 because it interacts with two catalytic residues, Glu166, and the S1/S2 subsites, which are the key elements for the recognition of substrates [51, 52]. Our results shows a binding score of -8.90 ± 0.01 kcal/mol for amentoflavone-Nsp5 complex; this value is comparable with other studies which report similar interacting residues and binding scores of -7.589 kcal/mol (PDB ID: 6WNP) [53], -9.4 kcal/mol (PDB ID: 6M2N) [49], -9.2 kcal/mol (PDB ID: 6LU7) [54], -27.0441 kcal/mol (PDB ID: 6LU7) [55], -9.6 kcal/mol (PDB ID: 6LU7) [56], -8.9 kcal/mol (protein modeled in Swiss Modeler) [57], -10.2 kcal/mol (PDB ID: 6LU7) [58], and -10.0 kcal/mol (PDB ID: 6LU7) [59].

Furthermore, inhibition of Nsp12 or RdRp could target its conserved polymerase motifs, highlighting motif A composed of residues from 611 to 626, including Asp618 important for the binding process. And motif C, which comprises residues from 753 to 767, includes the catalytic residues Ser759, Asp760, and Asp761 [21]. As Fig. 6J show, amentoflavone forms hydrogen bonds with Asp618, Asp623, Arg624, and Thr556, necessary for binding and stabilizing ligand within motif A and C; π-ion interactions with Lys621 and Asp760 create an electrostatic potential into the cavity, disfavoring electronic-based processes carried out by Nsp12. Besides the aforementioned interactions, it is also important to highlight those forms with Asp618 and Asp760, essential residues for catalytic site activity. Similar interactions are presented for AT9 binding (Fig. 6K), highlighting those with Lys621 and Arg624, necessary for binding and stabilizing; in addition, the guanine-like group occupies the site which recognizes the DNA strand [21]. Therefore, amentoflavone may be an excellent candidate to inhibit the Nsp12. Similar results have been published, reporting binding scores of -9.4 kcal/mol (protein modeled in Swiss Modeler) [57] and -9.3 kcal/mol (PDB ID: 6M71) [48].

Finally, Nsp15 or NendoU is associated with multiple functions and could be involved in allowing the virus to evade the immune system innate response by hiding the viral RNA from the macrophage dsRNA sensors [60]; the catalytic site of this protein is composed of the residue triad His235, His250, and Lys290. These amino acids have been demonstrated to be conserved in all viruses of the coronavirus family [61]. They are fundamental for the activity of the Nsp15 enzyme and the formation of its hexameric quaternary structure [62]. Our results, presented in Figs. 5A and 6L, show that amentoflavone interacts with His235 with a hydrogen bond, which is fundamental in substrate hydrolysis and complex stabilization, also supported by hydrogen bonds with Gln245, Val292, Ser294, and Thr341; moreover, this flavonoid forms hydrophobic interactions with Lys290 (part of the catalytic triad), Cys291, Tyr343, and Leu346, amino acids that serve as an anchor, promoting the binding

and residence of the substrate onto the catalytic site, favored by the aromatic rings of amentoflavone. From these interactions, we must distinguish those with Ser294 and Tyr343 because these residues together are believed to govern U specificity, in RNase A base recognition [63]. Similar interactions were observed for tipiracil (Fig. 6M), highlighting the recognition of carbonyl group by Ser294, which is specific for uracil recognition. With the information analyzed above, Nsp15 is another protein that could be inhibited by amentoflavone.

Ligand efficiency

Ligand efficiency (*LE*) allows us to compare molecules according to their average binding energy [59]; very low values indicate that the compound binds tightly to the protein. *LE* represents the average binding energy per non-hydrogen atom, where fair values of *LE* for inhibitors candidates are $LE > 0.3$ kcal [31]. Considering this information, for all the evaluated proteins, amentoflavone has ligand efficiency values less than 0.3 kcal (0.23, 0.20, and 0.18 for Nsp1 clusters, 0.22 for Nsp3, 0.21 and 0.23 for Nsp5 clusters, 0.23 for Nsp12, and 0.23 for Nsp15), information that supports the proposal of using this flavonoid as a potential inhibitor of non-structural proteins of the SARS-CoV-2 virus. These values are smaller than those of the co-crystalized ligands, i.e., GRL0617 0.33, baicalein 0.34 and 0.35, and tipiracil 0.35, except for AT9 (0.22). In the same sense, amentoflavone exhibits low theoretical dissociation constants (*Kd*) for each of the evaluated proteins, reaffirming the stability of the complex and the favorable binding of the ligand, even promising a most efficient inhibitor of these non-structural proteins (fewer doses are required for reaching the inhibitory effect). The top 10 molecules interacting with the best docking scores for the selected clusters of each protein were selected for this comparison (Table S1).

Protein–ligand molecular dynamics

RMSD analysis

After evaluation of the three clusters of Nsp1-amentoflavone complex (Figure S1A, S2A and S3A), we can appreciate that for cluster 1 RMSD has the same behavior as the protein alone, just with a little high nm, due to the ligand binding; the ligand reaches its stability at 25 ns. More variations in ligand RMSD are observed for cluster 2, those sudden movements reflect on the global RMSD, mainly in the first 15 ns. Finally, about the third cluster, at the first ns of the complex RMSD has higher values than just protein caused by the fluctuations on ligand's RMSD. In this sense, the first cluster of Nsp1-amentoflavone complex is the most stable, and the three represent three different stages of the protein behavior.

With respect to Nsp3 (Figure S4A and S5A), complex and protein have no significant differences, in both amentoflavone and GLR-0617, due to the stability of the ligand which does not suddenly elevate the RMSD values. Also, protein, ligand, and the complex reach their best conformation at 18 ns, keeping its flexibility near the RMSD mean value (0.35 nm); the little variations in RMSD of the ligand let us to find different complex clusters.

On the other hand, the RMSD of cluster 1 of Nsp5-amentoflavone (Figure S6A) has no significative variations between complex and single protein, regarding ligand, two possible states could be identified with approximately 0.05 nm of difference; cluster 2 (Figure S7A) shows higher variation in complex against protein, this is due to the rise of RMSD values of the ligand. Similarly, the second cluster of Nsp5-baicalein complex (Figure S9A) shows a significant variation of protein vs. complex, which correlates with the ligand fluctuation. First cluster (Figure S8A) shows no variation in RMSD of complex vs. protein, the ligands show a lot of fluctuations along the whole trajectory, but two probable states can be defined based on this.

Talking about nsp12 (Figure S10A), amentoflavone reaches a single conformation at 17 ns, fluctuations of the ligands have significant influence on the RMSD of the complex; the behavior of the Nsp12-inhibitor is contrary to that shown for AT9 (Figure S11A), because variations of complex, ligand and protein maintain on the 0.18 nm average RMSD.

Finally, for the Nsp15, respecting to the complex with amentoflavone (Figure S12A), the RMSD of the complex have several variations, these variations could be a result of the high flexibility of the protein or for a high or they could be a result of several conformation changes because of ligand binding, although ligand has a very stable RMSD, representing its permanence into the binding site. In contrast, Nsp15 in complex with tipiracil (Figure S13A) has sudden variations at 65 to 80 ns, representing an interesting cluster for this complex.

Hydrogen bond analysis

The hydrogen bonds that form during the drug-receptor interaction are characteristic of a high-affinity binding; this is due to the force exerted by this bond repelling the force exerted by water in the cavities, conferring greater stability to the complex [63]. In other words, this approach allows us to have a closer look at the complete phenomenon, because in MD simulations during the formation of hydrogen bonds, it necessarily implies an energetic process of desolvation of the hydrogen bonds previously formed between the protein-water system [64].

Regarding the formation of hydrogen bonds, during all MD simulations, the amentoflavone establishes a variable

number of them with various residues of the SARS-CoV-2 Nsps. Throughout the simulation in the trajectories of the three trajectories of Nsp1 (Figure S1B, S2B and S3B), amentoflavone formed 2 hydrogen bonds on average and up to 5 for Nsp3 (Figure S4B) and Nsp15 (Figure S12B). The amentoflavone in complex with Nsp12 (Figure S10B) was able to form 5 hydrogen bonds in most of their conformations along the trajectory, in contrast with the co-crystallized ligand that formed up to 10 hydrogen bonds in the most of nanoseconds along the whole trajectory (Figure S11B). Finally, talking about Nsp15 for both amentoflavone and tipiracil, they reach a maximum of five hydrogen bonds, although there are ns with no hydrogen bonding, the permanence of ligands into binding pockets depend on hydrophobic interactions (Figure S12B and S13B).

Cluster analysis

The clustering process allows us to analyze the conformational behavior of the protein under conditions established on the MD simulations to find the most repeated conformation and thus the most representative protein–ligand binding process. In the following analysis, we have selected the most frequent, also representative, cluster from the best three of all five ligand–protein MD simulations (Fig. 7).

In Figs. 8, 9, 10, 11, and 12, we can see the 2D and 3D best cluster for each complex representation. For Nsp1 cluster 1 (Fig. 8A), we appreciate two interactions that had also been formed in the previous docking assay analysis with residues Trp161, forming two π-π interactions with two different rings of amentoflavone; a more stable anchor is formed by the π interactions with Phe157 and Ser167. We can also

see another hydrophobic carbon-hydrogen interaction with the residue Gly168 and another hydrogen bond with Gln158. In the case of cluster 2 (Fig. 8B), the main interactions are hydrophobic, i.e., carbon-hydrogen and π interactions, with Leu4, Val5, Leu145, Gly146, and Thr151, highlighting the only hydrogen bond with Leu149. Referring to cluster 3 (Fig. 8C), it is the poorest talking in interactions terms as it just has two interactions: a hydrogen bond with Ser40 and a π-alkyl with Leu140. By these, the most representative way of binding on the well described pocket is cluster 1.

In the Nsp3 cluster binding site, amentoflavone (Fig. 9A) remains into the binding pocket, keeping all interactions of previous performed docking, highlighting those with Asp164, important for ligand stabilization; Tyr268 presumed to make a fitting induced movement to adopt a closer conformation and with Arg166 and Glu167, important for water and carbonyl coordination [46, 47]. Regarding to the inhibitor GRL0617 (Fig. 9B), this compound preserves π-π interactions with Tyr268 and hydrophobic π interactions with Pro247, Pro248, and Tyr264, residues within the site called the flexible loop BL2 or β-turn [44, 47], preserving that with Pro248 as in the docking assay.

For Nsp5, it can be observed that amentoflavone at cluster 1 (Fig. 10A) that the previous docking reported interactions are not preserved, instead hydrogen bonds are formed with Gly138 and Glu288, also π interactions with Tyr126 and Lys137 are included. In comparison with cluster 2 (Fig. 10B), just one interaction is preserved: Tyr126, and new ones are formed with residues near to Tyr126 (which seems to be crucial in the binding process of amentoflavone): Val114, Gln128, Cys128, Ser139, and Leu141, residues considered important for ligand recognition [65], and

Fig. 7 Results of cluster analysis of the molecular dynamics of the five Nsp-ligand complexes
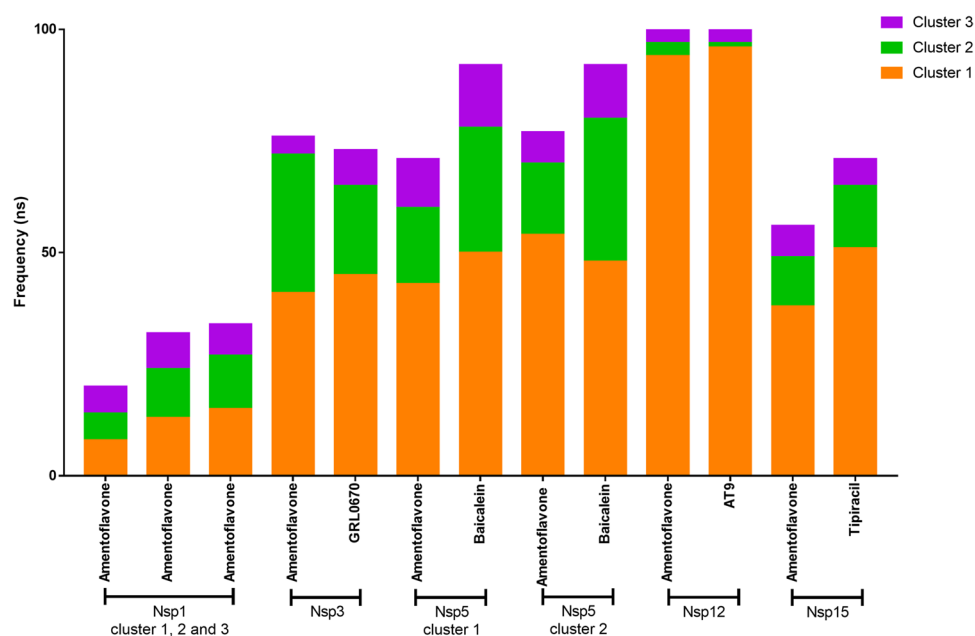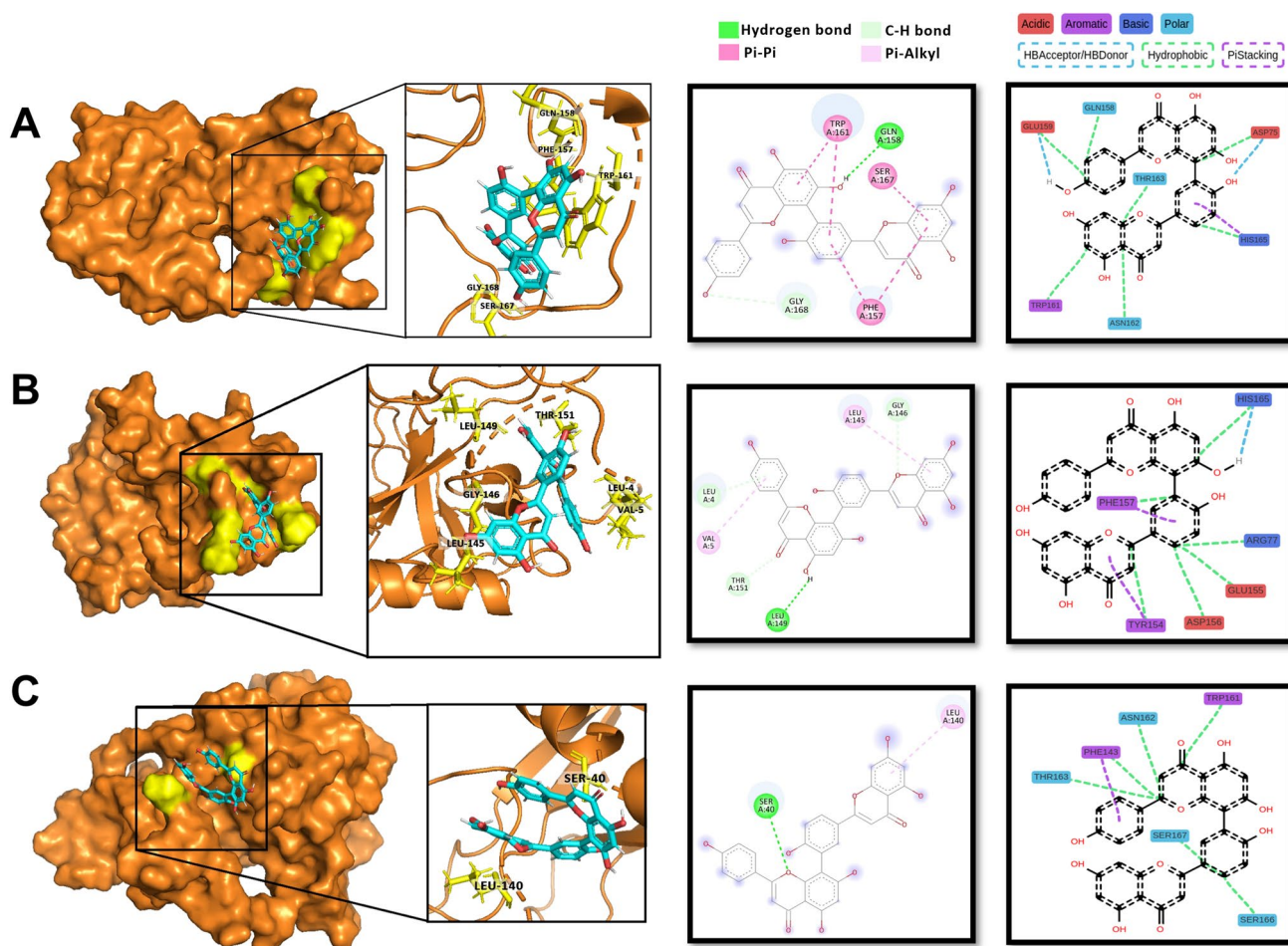
Fig. 8 3D and 2D models of the amentoflavone onto the most favorable cluster in complex with the three clusters of Nsp1 and their interaction fingerprint along whole dynamics

important for binding of other molecules with inhibitory activity, such as paritaprevir, lopinavir, and epigallocatechin-3-gallate [66]. In contrast, baicalein in both clusters (Fig. 10C and D), binds with less amino acids, totally different to those reported in docking assay: Gln19, Met49, and Gly120 for cluster 1 and for cluster 2, baicalein interacts with amino acids of the catalytic site: His41 and Cys145, reaffirming the mechanisms of inhibition of this flavone; complemented with the hydrophobic interactions of Met49, Leu50, Met165, and Ala191; also highlighting the hydrogen bond with Glu166.

Regarding the Nsp12 cluster, amentoflavone (Fig. 11A) remained at the binding site keeping the interactions reported in the docking assay such as Ala547, Arg555, and Asp760, the last one, essential for catalytic site activity (as mentioned above); additionally, interactions with Asp845 and Lys545 were formed, which have already been reported as capable of binding to at least three other drugs with inhibitory potential [67, 68]. On the other hand, AT9 (Fig. 11B) maintains in the binding site, very favorable by

the phosphate groups of its structure (as mentioned above), most of the interactions of this cluster are preserved from the docking assay, highlighting electrostatic interactions with Lys551, Arg555, Lys621, and Arg624, reaffirming its mechanism as mimic of uracil.

Finally, in the cluster obtained from the amentoflavone-Nsp15 complex trajectory (Fig. 12A), we observed that the same hydrogen bonds formed in the docking performed prior MD simulation with residues His235, Ser294, and Tyr343, as well as π-π interactions with residues Trp333 and Tyr343. In addition to these interactions, here, the flavonoid forms a new hydrogen bond with the Glu340 residue. All these interactions remain within the binding site of known inhibitors, such as benzopurpurin 4B, which, in addition to sharing the same interactions shown here, has also been shown to inhibit Nsp15 in vitro [69]. In the case of tipiracil, it keeps into the binding pocket by interacting strongly with Glu267 by a salt bridge and π-π interactions of guanidine ring with Phe280 (Fig. 12B).
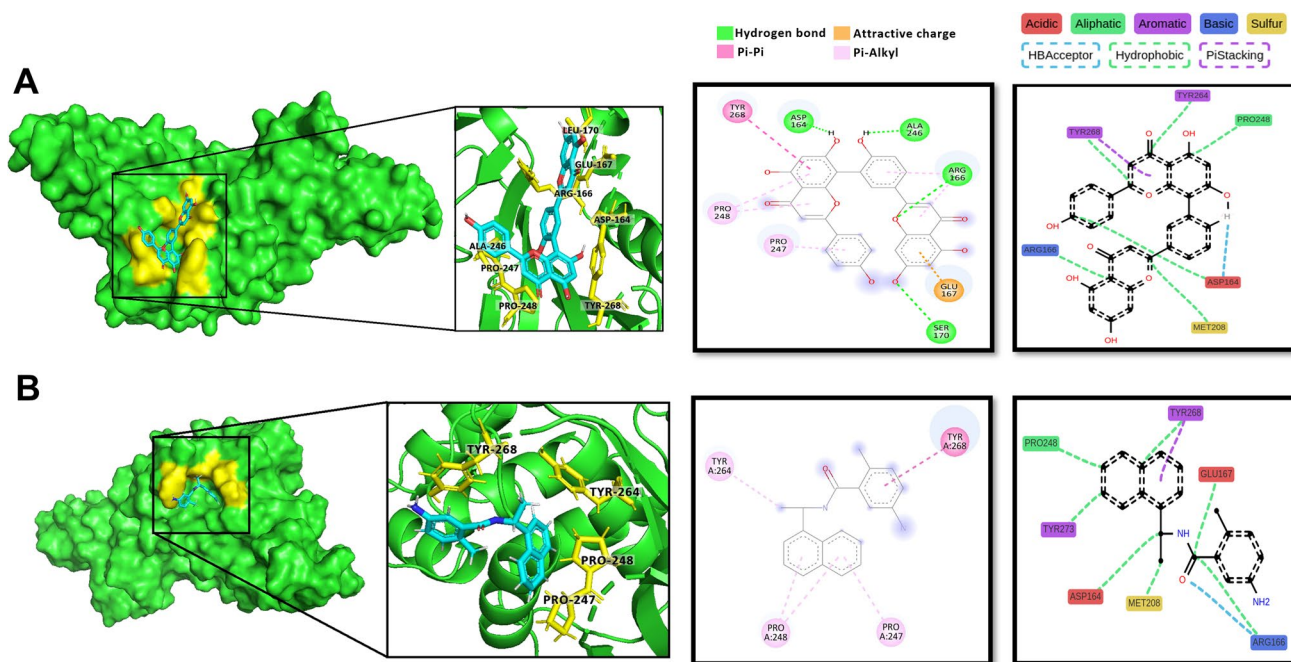
Fig. 9 3D and 2D models of the amentoflavone and GRL0617 onto the most favorable cluster in complex with the three clusters of Nsp3 and their interaction fingerprint along whole dynamics

Protein–ligand fingerprint

The time that protein–ligand interactions maintain along the 100 ns of molecular dynamics simulation are represented in Fig. 4E, 5, 6, 7, 8, 9, 10, 11, 12. Analyzing the interactions of amentoflavone with the three clusters of Nsp1, we can appreciate that most of the time the main amino acids that keep the ligand at binding site are Trp161, Phe157, Gln158, His165, and Gly168, mainly through hydrophobic interactions (Fig. 8A); at the cluster 2 (Fig. 8B), which conformation displace some armstrongs the ligand, the main residues interacting with amentoflavone are Leu149, Asn128, Thr151, Asp144, and Gly150, by hydrophobic and hydrogen bonding, interestingly, the interactions with Phe157 and His165 diminished; at the end, amentoflavone interacts mostly via hydrophobic with Leu140, Gly146, Leu145, Glu148, and Leu149 in cluster 3 (Fig. 8C). By this way, amentoflavone binds into the hydrophobic cavity formed by α1 and α2 helices of Nsp1, which is confirmed by the residues between Asp148 and Gly180, important for the 40S ribosomal subunit binding [41].

Regarding Nsp3, the main reported interactions into the binding site involve Asp164, Gln269 with hydrogen bonds, and Tyr264, Tyr268, Pro247, Pro248, Thr301, Arg166 with aromatic interactions, mainly in the flexible loop BL2 or β-turn, an important mobile loop (Gly266–Gly271) [44, 47]. Amentoflavone remains in the binding site due to the interactions formed by Ser293, Tyr296, Lys297, Lys292,

and Tyr264 mainly by hydrophobic and hydrogen bonding (Fig. 9A), fitting perfect with the flexible loop BL2 and the specific site for leucine side chain of LXGG consensus sequence recognition [44], for PLPro proteolytic cleavage activity. Similarly, GRL0617 interacts mainly with Tyr268, Tyr264, Pro247, Met208, and Pro248 (Fig. 9B).

In the same sense, Nsp5 hydrophobic interactions are the main type formed along the whole molecular dynamics, for both amentoflavone and baicalein. In case of amentoflavone, the five main residues for cluster 1 (Fig. 10A) includes Tyr126, Gly138, Ser139, Lys137, and Gln127; two of these amino acids are conserved for the cluster 2: Tyr126, Ser139 (Fig. 10B), complemented by the interactions with Tyr118, Phe140, and Cys128. Based on this information, we can mention that amentoflavone accommodates into the binding cavity, nevertheless, it does not reach the catalytic dyad residues, but the occupancy of the binding pocket mediated by the hydrophobic and π-stacking interactions with Tyr126 and Phe140, suggesting that the inhibition mechanism is through binding site competition and occupation instead electronic disruption of catalytic dyad. In contrast, baicalein forms mostly hydrophobic and π-stacking interactions with the residues His41 and Cys145, in both clusters (Fig. 10C and D), complemented by the interactions with the surrounding subsites, indicating that the main mechanism of this molecule is by disruption of the catalytic reaction.

On the other hand, the evaluated known antagonist (AT9) of Nsp12 (Fig. 11B) binds favorably into the
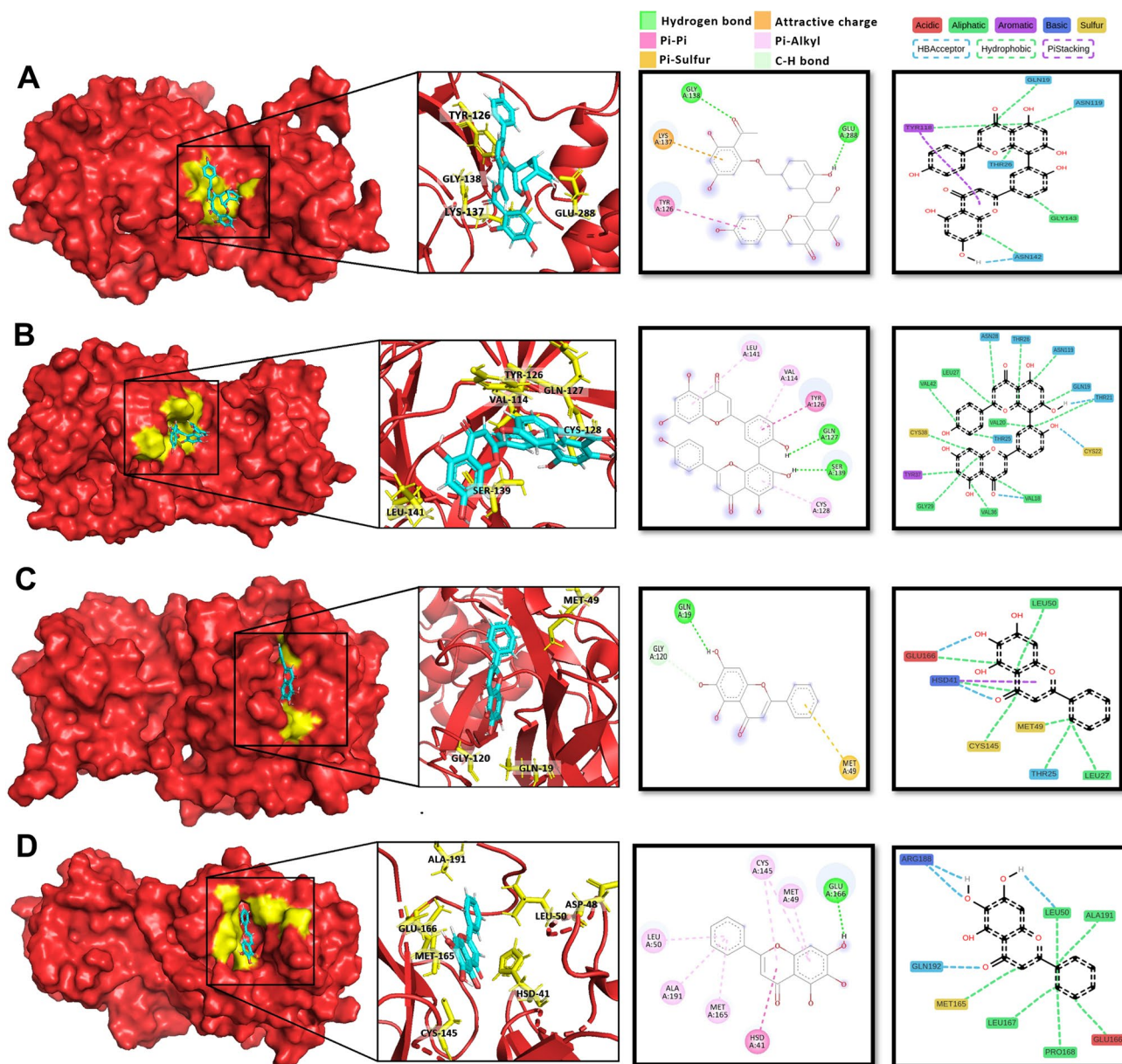
Fig. 10 3D and 2D models of the amentoflavone and baicalein onto the most favorable two clusters in complex with the three clusters of Nsp5 and their interaction fingerprint along whole dynamics

binding pocket by electrostatic interactions such as anionic and hydrogen bonds with Arg566, Arg497, Lys563, and Lys493, provoked by the phosphate groups contain; in contrast mostly of the interactions between amentoflavone and Nsp12 (Fig. 11A) are hydrophobic and in some cases are hydrogen bonds. The main residues which favor the binding are Arg497, Asp787, Ile789, Val409, and Asp702. In both cases, the compounds occupy the main entrance of DNA coupling; the advantage of AT9 is that it possesses a couple of phosphate groups which mimics those that nucleic acid possess.

Finally, in the case of Nsp15 the interactions that favor the amentoflavone binding (Fig. 12A) and permanence into the binding pocket are with Gly152, Lys151, Val188, Gln246, and Val293. Although the amino acids of the catalytic triad interact with the ligand, but not for all the time of molecular dynamics, the interaction with surrounding residues lets us to propose that the inhibition method of amentoflavone is by the rearrangement of the binding pocket, leading to no catalytic reaction, supported by hydrophobic and hydrogen bonding. In the same way, tipiracil (Fig. 12B) keeps on the binding pocket, with no
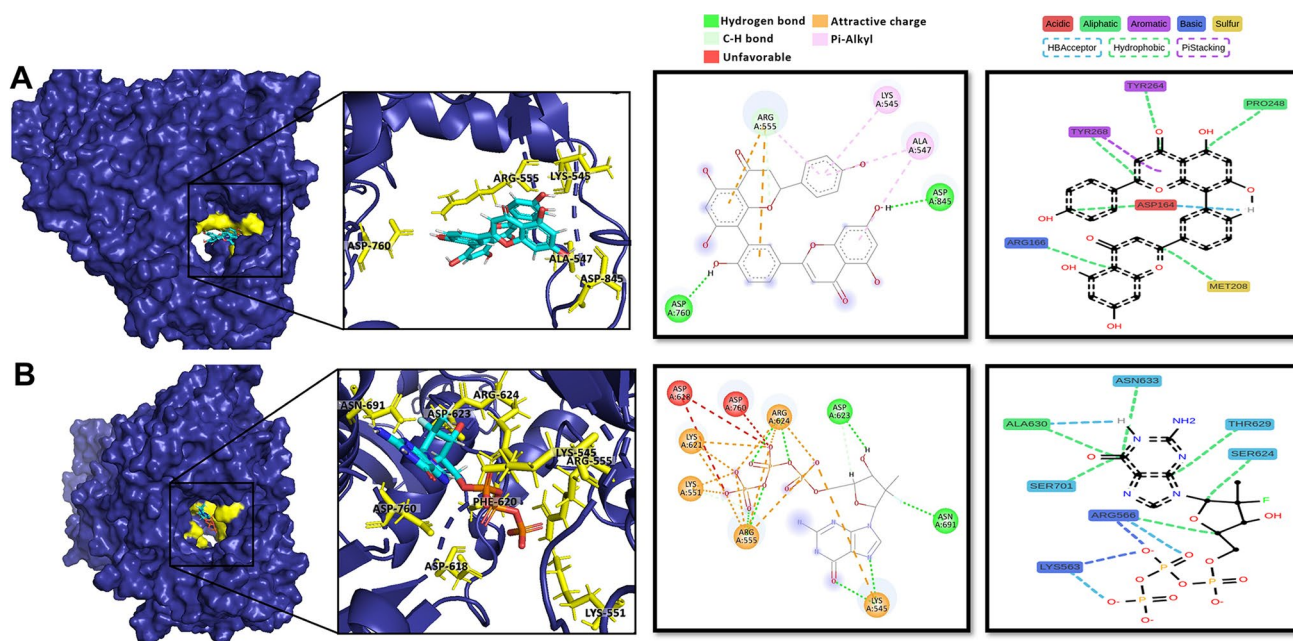
Fig. 11 3D and 2D models of the amentoflavone and AT9 onto the most favorable cluster in complex with the three clusters of Nsp12 and their interaction fingerprint along whole dynamics
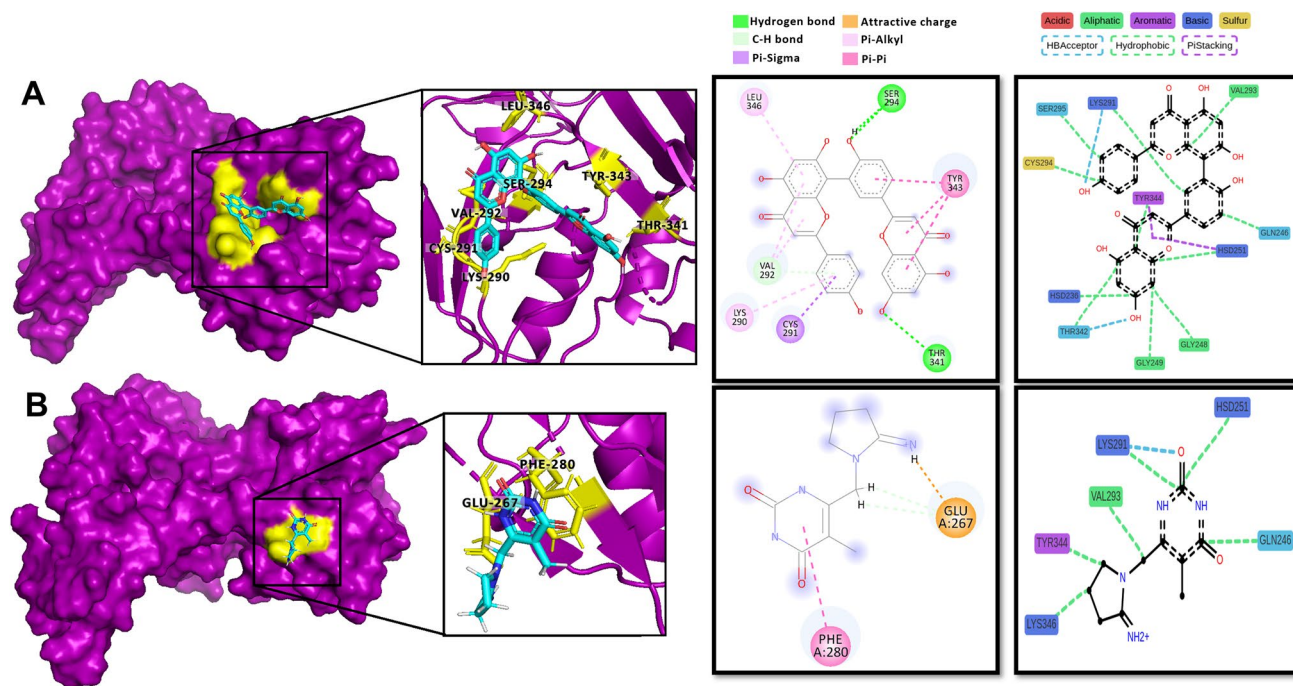

Fig. 12 3D and 2D models of the amentoflavone and tipiracil onto the most favorable cluster in complex with the three clusters of Nsp15 and their interaction fingerprint along whole dynamics

direct interaction with the catalytic residues, but interacting with surrounding amino acids like Tyr344, Val293, Lys291, His251, and Ser295, mainly with hydrophobic and electrostatic interactions.

Electrostatics and van der Waals energies

Contributions of electrostatic and van der Waals interactions to global binding energy play a major role in determining

protein–ligand binding specificity and the rate of protein–ligand association [70]. Regarding to the calculated energies for the three clusters of Nsp1 (Figure S1C, Figure S2C and Figure S3C) in complex with amentoflavone, most of the contribution to the global binding energy is mediated by van der Waals, correlating to hydrophobic interactions reported in the above section, moreover at some times of the trajectory, electrostatic energy contributes in a greater manner (~ 25 and 50 ns), correlating with electronic π interactions.

Regarding Nsp3, a curious behavior because there are some moments in the trajectory that electrostatic energy does not contribute to the binding process (Figure S4C and Figure S5C), and the van der Waals contributions seems to be zero; this could be provoked by no residue-ligand interaction or for a remoteness of the ligand from its position. Apart from this curious fact, the co-crystallized ligand (Figure S5C) of Nsp3 binding is mediated by the contributions of van der Waals energy, in difference with amentoflavone (Figure S4C) which contributions are equative between electrostatic and hydrophobic, as correlated with the analysis of interaction fingerprint.

In a similar way, most of the contribution to global binding energy of the Nsp5-ligand complexes is derived from van der Waals; nevertheless, there are several nanoseconds where electrostatic energies contribute in a higher way, principally at the middle and the first quarter of simulation. These contributions are reflected into the interaction type that establishes each compound with residues of the binding pocket, which are mainly hydrophobic, and those peaks of electrostatic contributions correlate well with π-stacking interactions and hydrogen bonding. These results are similar between both clusters (Figure S6C-S7C and Figure S8C-S9C).

Regarding Nsp12 and amentoflavone (Figure S10C), at least half of the simulation time the electrostatic energy contributes more than van der Waals to the binding process, energies that correlates with the hydrogen bonding of Asp787, Asp702, and Arg497 and the hydrophobic interactions. In the case of AT9 (Figure S11C), electrostatic interactions contribute abysmally to the global binding constant (-1100 kJ/mol); this correlates perfectly with the fully anionic and hydrogen bonding observed in the interaction fingerprint.

Finally, respecting to Nsp15, there are several moments, for both ligands, that energy contribution is zero (Figure S12C and S13C); it seems to be that only residual van der Waals energy remains. This phenomenon could be due to a displacement of ligand form the initial position, nevertheless, the RMSD values from both remain stable, so no correlation could be established between with the two variables, but yes with hydrogen bonding; nevertheless, the binding process is favored by other class of hydrophobic interactions.

SASA

Solvent-accessible surface area (SASA) is an important descriptor in ligand binding. The extent of ligand SASA value decreases upon binding indicates whether the ligand is deeply buried or not upon binding to the pocket. For all complexes (Figure S1D-S13D), SASA dynamic behavior suggests preferential confinement of the different ligands within the protein pocket, although Nsp15 is the one with the most variability in the area (~ 15 nm^2), the rest of them just vary in ~ 15 nm^2 from the mean SASA value.

Conclusion

The main idea of this work was to find a natural compound that could bind five different non-structural proteins of SARS-CoV-2 in order to stop virus infection by inhibition of key process targets, although finding a single target is a good option for the inhibition viral disease, a multitarget approach, as presented in this work, has some advantages such as inhibition mechanisms are multiple, combination with other drugs could lead to synergic effect, and multidrug assessment could be avoided.

In this way, amentoflavone was selected, among 478 flavonoids, as a multitarget inhibitor for being the only flavonoid capable of binding to the five non-structural proteins of SARS-CoV-2 (Nsp1, Nsp3, Nsp5, Nsp12, and Nsp15). We demonstrate with MD simulations high stability of the complex formed between the amentoflavone and the five Nsps throughout the 100-ns simulation. Furthermore, the information provided by the energy analysis showed that in order of affinity and efficacy, amentoflavone would have a greater capacity to inhibit Nsp5, followed by Nsp12, Nsp15, Nsp3, and finally Nsp1. Allowing us to emphasize that amentoflavone has the potential to function as a multitarget molecule. Nevertheless, due to the in silico approach, some of the variables influencing the binding process in vitro and in vivo could be avoided, so biological experiments are needed to corroborate the phenomena described here.

were performed by Andrés Portilla-Martínez and Miguel Ortiz-Flores. Investigation, formal analysis, and results validation were performed by Cristian Gonzalez-Ruiz and Isabel Hidalgo. Supervision, project administration, and provision of resources were performed by Nayelli Nájera, Eduardo Meaney, and Guillermo Ceballos. The first draft of the manuscript was written by Miguel Ortiz-Flores and Andrés Portilla-Martínez and all authors commented on previous versions of the manuscript. Review and editing of the final version were performed by Nayelli Nájera and Guillermo Ceballos. All authors read and approved the final manuscript.

Declarations

Conflict of interest Dr. Ceballos is a stockholder of Epirium, Inc.

References

1. World Health Organization (2022) WHO COVID-19 dashboard. In: https://covid19.who.int/

2. He F, Deng Y, Li W (2020) Coronavirus disease 2019: what we know? J Med Virol 92:719–725. https://doi.org/10.1002/jmv.25766

3. Bhavana V, Thakor P, Singh SB, Mehra NK (2020) COVID-19: pathophysiology, treatment options, nanotechnology approaches, and research agenda to combating the SARS-CoV2 pandemic. Life Sci 261:118336. https://doi.org/10.1016/j.lfs.2020.118336

4. Izda V, Jeffries MA, Sawalha AH (2021) COVID-19: a review of therapeutic strategies and vaccine candidates. Clin Immunol 222:108634. https://doi.org/10.1016/j.clim.2020.108634

5. Brüssow H (2021) COVID-19: vaccination problems. Environ Microbiol 23:2878–2890. https://doi.org/10.1111/1462-2920.15549

6. Giovanetti M, Benedetti F, Campisi G et al (2021) Evolution patterns of SARS-CoV-2: snapshot on its genome variants. Biochem Biophys Res Commun 538:88–91. https://doi.org/10.1016/j.bbrc.2020.10.102

7. Rezagholizadeh A, Khiali S, Sarbakhsh P, Entezari-Maleki T (2021) Remdesivir for treatment of COVID-19; an updated systematic review and meta-analysis. Eur J Pharmacol 897:173926. https://doi.org/10.1016/j.ejphar.2021.173926

8. Sahebnasagh A, Avan R, Saghafi F et al (2020) Pharmacological treatments of COVID-19. Pharmacol Rep 72:1446–1478. https://doi.org/10.1007/s43440-020-00152-9

9. Rohaim MA, el Naggar RF, Clayton E, Munir M (2021) Structural and functional insights into non-structural proteins of coronaviruses. Microb Pathog 150:104641. https://doi.org/10.1016/j.micpath.2020.104641

10. Ross JA, Kasum CM (2002) Dietary flavonoids: bioavailability, metabolic effects, and safety. Annu Rev Nutr 22:19–34. https://doi.org/10.1146/annurev.nutr.22.111401.144957

11. Russo M, Moccia S, Spagnuolo C, et al (2020) Roles of flavonoids against coronavirus infection. Chem Biol Interact 328:. https://doi.org/10.1016/J.CBI.2020.109211

12. Yu S, Yan H, Zhang L, et al (2017) A review on the phytochemistry, pharmacology, and pharmacokinetics of amentoflavone, a naturally-occurring biflavonoid. Molecules 22:. https://doi.org/10.3390/MOLECULES22020299

13. Cai J, Zhao C, Du Y, et al (2019) Amentoflavone ameliorates cold stress-induced inflammation in lung by suppression of C3/BCR/NF-κB pathways. BMC Immunol 20:. https://doi.org/10.1186/S12865-019-0331-Y

14. Zhang Z, Sun T, Niu JG et al (2015) Amentoflavone protects hippocampal neurons: anti-inflammatory, antioxidative, and antiapoptotic effects. Neural Regen Res 10:1125–1133. https://doi.org/10.4103/1673-5374.160109

15. Hwang IS, Lee J, Jin HG et al (2012) Amentoflavone stimulates mitochondrial dysfunction and induces apoptotic cell death in Candida albicans. Mycopathologia 173:207–218. https://doi.org/10.1007/S11046-011-9503-X

16. Rong S, Wan D, Fan Y, et al (2019) Amentoflavone affects epileptogenesis and exerts neuroprotective effects by inhibiting NLRP3 inflammasome. Front Pharmacol 10:. https://doi.org/10.3389/FPHAR.2019.00856

17. Qin L, Zhao Y, Zhang B, Li Y (2018) Amentoflavone improves cardiovascular dysfunction and metabolic abnormalities in high fructose and fat diet-fed rats. Food Funct 9:243–252. https://doi.org/10.1039/C7FO01095H

18. Zheng W, Zhang C, Li Y et al (2021) Folding non-homologous proteins by coupling deep-learning contact maps with I-TASSER assembly simulations. Cell Reports Methods 1:100014. https://doi.org/10.1016/j.crmeth.2021.100014

19. Ma C, Sacco MD, Xia Z et al (2021) Discovery of SARS-CoV-2 papain-like protease inhibitors through a combination of high-throughput screening and a FlipGFP-based reporter assay. ACS Cent Sci 7:1245–1260. https://doi.org/10.1021/acscentsci.1c00519

20. Su H, Yao S, Zhao W et al (2020) Anti-SARS-CoV-2 activities in vitro of Shuanghuanglian preparations and bioactive ingredients. Acta Pharmacol Sin 41:1167–1177. https://doi.org/10.1038/s41401-020-0483-6

21. Gao Y, Yan L, Huang Y et al (1979) (2020) Structure of the RNA-dependent RNA polymerase from COVID-19 virus. Science 368:779–782. https://doi.org/10.1126/science.abb7498

22. Kim Y, Wower J, Maltseva N et al (2021) Tipiracil binds to uridine site and inhibits Nsp15 endoribonuclease NendoU from SARS-CoV-2. Communications Biology 4:193. https://doi.org/10.1038/s42003-021-01735-9

23. Burley SK, Bhikadiya C, Bi C et al (2021) RCSB Protein Data Bank: powerful new tools for exploring 3D structures of biological macromolecules for basic and applied research and education in fundamental biology, biomedicine, biotechnology, bioengineering and energy sciences. Nucleic Acids Res 49:D437–D451. https://doi.org/10.1093/nar/gkaa1038

24. Pettersen EF, Goddard TD, Huang CC et al (2004) UCSF Chimera? A visualization system for exploratory research and analysis. J Comput Chem 25:1605–1612. https://doi.org/10.1002/jcc.20084

25. Morris GM, Huey R, Lindstrom W et al (2009) AutoDock4 and AutoDockTools4: automated docking with selective receptor flexibility. J Comput Chem 30:2785–2791. https://doi.org/10.1002/jcc.21256

26. Kanehisa M (2000) KEGG: Kyoto Encyclopedia of Genes and Genomes. Nucleic Acids Res 28:27–30. https://doi.org/10.1093/nar/28.1.27

27. Shannon A, Fattorini V, Sama B et al (2022) A dual mechanism of action of AT-527 against SARS-CoV-2 polymerase. Nat Commun 13:621. https://doi.org/10.1038/s41467-022-28113-1

28. O'Boyle NM, Banck M, James CA et al (2011) Open Babel: an open chemical toolbox. Journal of Cheminformatics 3:33. https://doi.org/10.1186/1758-2946-3-33

29. Trott O, Olson AJ (2009) AutoDock Vina: improving the speed and accuracy of docking with a new scoring function, efficient

optimization, and multithreading. J Comp Chem NA-NA. https://doi.org/10.1002/jcc.21334

30. BIOVIA DS (2022) Discovery Studio, 2017R2

31. Abad-Zapatero C (2007) Ligand efficiency indices for effective drug discovery. Expert Opin Drug Discov 2:469–488. https://doi.org/10.1517/17460441.2.4.469

32. Abraham MJ, Murtola T, Schulz R et al (2015) GROMACS: high performance molecular simulations through multi-level parallelism from laptops to supercomputers. SoftwareX 1–2:19–25. https://doi.org/10.1016/j.softx.2015.06.001

33. Berendsen HJC, van der Spoel D, van Drunen R (1995) GROMACS: a message-passing parallel molecular dynamics implementation. Comput Phys Commun 91:43–56. https://doi.org/10.1016/0010-4655(95)00042-E

34. Lemkul JA (2018) From proteins to perturbed Hamiltonians: a suite of tutorials for the GROMACS-2018 molecular simulation package, v1.0. Living J Comp Mol Sci 1(1):5068

35. Schrodinger LLC (2015) The PyMOL Molecular Graphics System, version 1.8

36. Bouysset C, Fiorucci S (2021) ProLIF: a library to encode molecular interactions as fingerprints. Journal of Cheminformatics 13:72. https://doi.org/10.1186/s13321-021-00548-6

37. Mendez AS, Ly M, González-Sánchez AM et al (2021) The N-terminal domain of SARS-CoV-2 nsp1 plays key roles in suppression of cellular gene expression and preservation of viral gene expression. Cell Rep 37:109841. https://doi.org/10.1016/J.CELREP.2021.109841

38. Schubert K, Karousis ED, Jomaa A et al (2020) SARS-CoV-2 Nsp1 binds the ribosomal mRNA channel to inhibit translation. Nat Struct Mol Biol 27:959–966. https://doi.org/10.1038/S41594-020-0511-8

39. Shen Z, Zhang G, Yang Y, et al (2021) Lysine 164 is critical for SARS-CoV-2 Nsp1 inhibition of host gene expression. Journal of General Virology 102:. https://doi.org/10.1099/jgv.0.001513

40. Sakuraba S, Xie Q, Kasahara K et al (2022) Extended ensemble simulations of a SARS-CoV-2 nsp1–5'-UTR complex. PLoS Comput Biol 18:e1009804. https://doi.org/10.1371/journal.pcbi.1009804

41. Thoms M, Buschauer R, Ameismeier M et al (1979) (2020) Structural basis for translational shutdown and immune evasion by the Nsp1 protein of SARS-CoV-2. Science 369:1249–1255. https://doi.org/10.1126/science.abc8665

42. Mielech AM, Deng X, Chen Y et al (2015) Murine coronavirus ubiquitin-like domain is important for papain-like protease stability and viral pathogenesis. J Virol 89:4907–4917. https://doi.org/10.1128/JVI.00338-15

43. Ratia K, Saikatendu KS, Santarsiero BD et al (2006) Severe acute respiratory syndrome coronavirus papain-like protease: structure of a viral deubiquitinating enzyme. Proc Natl Acad Sci U S A 103:5717–5722. https://doi.org/10.1073/PNAS.0510851103

44. Osipiuk J, Azizi S-A, Dvorkin S et al (2021) Structure of papain-like protease from SARS-CoV-2 and its complexes with non-covalent inhibitors. Nat Commun 12:743. https://doi.org/10.1038/s41467-021-21060-3

45. Bhati S (2020) Structure-based drug designing of naphthalene based SARS-CoV PLpro inhibitors for the treatment of COVID-19. Heliyon 6:. https://doi.org/10.1016/J.HELIYON.2020.E05558

46. Báez-Santos YM, st. John SE, Mesecar AD, (2015) The SARS-coronavirus papain-like protease: structure, function and inhibition by designed antiviral compounds. Antiviral Res 115:21–38. https://doi.org/10.1016/j.antiviral.2014.12.015

47. Ratia K, Pegan S, Takayama J et al (2008) A noncovalent class of papain-like protease/deubiquitinase inhibitors blocks SARS virus replication. Proc Natl Acad Sci U S A 105:16119–16124. https://doi.org/10.1073/PNAS.0805240105

48. Nallusamy S, Mannu J, Ravikumar C, et al (2021) Exploring phytochemicals of traditional medicinal plants exhibiting inhibitory activity against main protease, spike glycoprotein, RNA-dependent RNA polymerase and non-structural proteins of SARS-CoV-2 through virtual screening. Front Pharmacol 12:. https://doi.org/10.3389/FPHAR.2021.667704

49. Swargiary A, Mahmud S, Saleh MA (2020) Screening of phytochemicals as potent inhibitor of 3-chymotrypsin and papain-like proteases of SARS-CoV2: an in silico approach to combat COVID-19. J Biomol Struct Dyn. https://doi.org/10.1080/07391102.2020.1835729

50. Cho E, Rosa M, Anjum R et al (2021) Dynamic profiling of β-coronavirus 3CL M^{pro} protease ligand-binding sites. J Chem Inf Model 61:3058–3073. https://doi.org/10.1021/acs.jcim.1c00449

51. Su H, Yao S, Zhao W, et al (2020) Discovery of baicalin and baicalein as novel, natural product inhibitors of SARS-CoV-2 3CL protease in vitro; bioRxiv 2020.04.13.038687. https://doi.org/10.1101/2020.04.13.038687

52. Tan J, Verschueren KHG, Anand K et al (2005) pH-dependent conformational flexibility of the SARS-CoV main proteinase (Mpro) dimer: molecular dynamics simulations and multiple X-ray structure analyses. J Mol Biol 354:25–40. https://doi.org/10.1016/j.jmb.2005.09.012

53. Patil R, Chikhale R, Khanal P, et al (2021) Computational and network pharmacology analysis of bioflavonoids as possible natural antiviral compounds in COVID-19. Inform Med Unlocked 22:. https://doi.org/10.1016/J.IMU.2020.100504

54. Ghosh R, Chakraborty A, Biswas A, Chowdhuri S (2020) Computer aided identification of potential SARS CoV-2 main protease inhibitors from diterpenoids and biflavonoids of Torreya nucifera leaves. J Biomol Struct Dyn. https://doi.org/10.1080/07391102.2020.1841680

55. Lokhande K, Nawani NK, Venkateswara S, Pawar S (2020) Biflavonoids from Rhus succedanea as probable natural inhibitors against SARS-CoV-2: a molecular docking and molecular dynamics approach. J Biomol Struct Dyn. https://doi.org/10.1080/07391102.2020.1858165

56. Varughese JK, Joseph Libin KL, Sindhu KS et al (2021) Investigation of the inhibitory activity of some dietary bioactive flavonoids against SARS-CoV-2 using molecular dynamics simulations and MM-PBSA calculations. J Biomol Struct Dyn. https://doi.org/10.1080/07391102.2021.1891139

57. Mahmoudi S, Balmeh N, Mohammadi N, Sadeghian-Rizi T (2021) The novel drug discovery to combat COVID-19 by repressing important virus proteins involved in pathogenesis using medicinal herbal compounds. Avicenna J Med Biotechnol 13:107–115. https://doi.org/10.18502/AJMB.V13I3.6370

58. Sawant S, Patil R, Khawate M, et al (2021) Computational assessment of select antiviral phytochemicals as potential SARS-Cov-2 main protease inhibitors: molecular dynamics guided ensemble docking and extended molecular dynamics. In Silico Pharmacol 9:. https://doi.org/10.1007/S40203-021-00107-9

59. Yañez O, Osorio MI, Areche C, et al (2021) Theobroma cacao L. compounds: theoretical study and molecular modeling as inhibitors of main SARS-CoV-2 protease. Biomedicine & pharmacotherapy = Biomedecine & pharmacotherapie 140:. https://doi.org/10.1016/J.BIOPHA.2021.111764

60. Deng X, Hackbart M, Mettelman RC et al (2017) Coronavirus nonstructural protein 15 mediates evasion of dsRNA sensors and limits apoptosis in macrophages. Proc Natl Acad Sci 114:E4251–E4260. https://doi.org/10.1073/pnas.1618310114

61. Krishnan DA, Sangeetha G, Vajravijayan S et al (2020) Structure-based drug designing towards the identification of potential anti-viral for COVID-19 by targeting endoribonuclease NSP15.

Informatics in Medicine Unlocked 20:100392. https://doi.org/10.1016/j.imu.2020.100392

62. Zhang L, Li L, Yan L, et al (2018) Structural and biochemical characterization of endoribonuclease Nsp15 encoded by Middle East respiratory syndrome coronavirus. Journal of Virology 92:. https://doi.org/10.1128/JVI.00893-18

63. Kim Y, Jedrzejczak R, Maltseva NI et al (2020) Crystal structure of Nsp15 endoribonuclease NendoU from SARS-CoV-2. Protein Sci 29:1596–1605. https://doi.org/10.1002/pro.3873

64. Ferreira De Freitas R, Schapira M (2017) A systematic analysis of atomic protein-ligand interactions in the PDB. Medchemcomm 8:1970–1981. https://doi.org/10.1039/c7md00381a

65. Hakami AR, Bakheit AH, Almehizia AA, Ghazwani MY (2022) Selection of SARS-CoV-2 main protease inhibitor using structure-based virtual screening. Future Med Chem 14:61–79. https://doi.org/10.4155/FMC-2020-0380

66. Farabi S, Saha N, Hasanuzzaman M et al (2020) Prediction of SARS-CoV-2 main protease inhibitors in medicinal plant-derived compounds by molecular docking approach. J Adv Biotechnol Exp Ther 3:79. https://doi.org/10.5455/jabet.2020.d159

67. Ur Rehman MF, Akhter S, Batool AI, et al (2021) Effectiveness of natural antioxidants against SARS-CoV-2? Insights from the in-silico world. Antibiotics (Basel) 10:. https://doi.org/10.3390/ANTIBIOTICS10081011

68. Adegbola PI, Fadahunsi OS, Adegbola AE, Semire B (2021) In silico studies of potency and safety assessment of selected trial drugs for the treatment of COVID-19. In Silico Pharmacol 9:. https://doi.org/10.1007/S40203-021-00105-X

69. Elhady SS, Abdelhameed RFA, Malatani RT, et al (2021) Molecular docking and dynamics simulation study of Hyrtios erectus isolated scalarane sesterterpenes as potential SARS-CoV-2 dual target inhibitors. Biology (Basel) 10:. https://doi.org/10.3390/BIOLOGY10050389

70. Kukić P, Nielsen JE (2010) Electrostatics in proteins and protein–ligand complexes. Future Med Chem 2:647–666. https://doi.org/10.4155/fmc.10.6

71. Chen D, Oezguen N, Urvil P, et al (2016) Regulation of protein-ligand binding affinity by hydrogen bond pairing. Science Advances 2:. https://doi.org/10.1126/sciadv.1501240